Pergamon

Cement and Concrete Research 29 (1999) 1705–1711

CEMENT AND CONCRETE RESEARCH

# Characterization of magnetite in silico-aluminous fly ash by SEM, TEM, XRD, magnetic susceptibility, and Mössbauer spectroscopy

S. Gomes[a,*], M. François[a], M. Abdelmoula[b], Ph. Refait[b], C. Pellissier[c], O. Evrard[a]

[a]*Laboratoire de Chimie du Solide Minéral, UMR CNRS 7555, Université Henri Poincaré, Nancy, BP 239, 54506 Vandoeuvre Cedex, France*
[b]*Laboratoire de Chimie Physique pour l'Environnement, UMR CNRS 7564, Université Henri Poincaré, Nancy, BP 239, 54506 Vandoeuvre Cedex, France*
[c]*EDF-CNET, les Collines de l'Arche, Cedex 24-92057 Paris la Défense, France*

Received 20 January 1999; accepted 7 June 1999

## Abstract

Spinel magnetite contained in a silico-aluminous fly ash (originating from la Maxe's power plant, near Metz in the east of France) issued from bituminous coal combustion has been studied by scanning and transmission electron microscopy linked with energy dispersive spectroscopy, X-ray diffraction, susceptibility measurements, and Mössbauer spectroscopy. The results show that in this magnetite Mg is strongly substituted for Fe and the chemical formula is closer to $MgFe_2O_4$ than $Fe_3O_4$. Magnetite also contains Mn, Ca, and Si elements, but at a lower proportion. The results are compatible with the chemical formula $Fe_{2.08}Mg_{0.75}Mn_{0.11}Ca_{0.04}Si_{0.02}O_4$ and crystallochemical formula $[Fe^{2+}_{0.92}Ca^{2+}_{0.06}Si^{4+}_{0.02}]^{tetra}[Fe^{3+}Fe^{2+}_{0.16}Mg^{2+}_{0.73}Mn^{2+}_{0.11}]^{octa}O_4$, showing the cation distribution on octahedral and tetrahedral sites of the spinel structure. The reason Mg element is not incorporated in soluble surface salt and in glass composition of the silico-aluminous fly ashes is now understood. 

*Keywords:* Fly ash; Characterization; TEM; X-ray diffraction; Magnetite

## 1. Introduction

Mineralogical properties of silico-aluminous fly ashes (material removed from coal power plants) are well known [1–12]. Their composition depends on the nature of the coal source, which can contain more or less calcium oxide. A bituminous coal usually gives rise to class F material (i.e., with low calcium content). Typically it consists of crystallized phases like α-quartz, mullite, hematite, and magnetite, in a matrix of aluminosilicate glass.

Whether the true chemical composition is linked to the structural properties of mullite and magnetite in such residues, usually designed by their classical chemical formula $(Al_2O_3)_3 \cdot (SiO_2)_2$ and $Fe_3O_4$, respectively, has not been studied. Indeed, contrarily to α-quartz, the composition of mullite and magnetite can vary and can incorporate many impurities. In this work, we were interested in studying magnetite especially. Another paper concerning mullite has already been submitted [13].

Magnetite has a spinel structure (space group Fd3m) $AB_2O_4$, $Z = 8$. Anions $O^{2-}$ on site 32e form a face-centered cubic network (FCC) where cations occupy 1/8 of the tetrahedral site (site 8a) lettered by A and half of the octahedral site (site 16d) lettered by B. Pure magnetite contains $Fe^{3+}$ on subnetwork A and equal quantities of $Fe^{2+}$ and $Fe^{3+}$ on subnetwork B. Thus, it is an inverse spinel that corresponds to the cristallochemical formula $[Fe^{3+}]^{tetra}[Fe^{3+},Fe^{2+}]^{octa}O_4$. The saturation magnetization $M_s$ is due to the influence of both networks A and B antiferromagnetically coupled. Since magnetic moments are 5 and 4 $\mu_B$ for $Fe^{3+}$ and $Fe^{2+}$, respectively, $M_s$ value for pure magnetite is 4 $\mu_B$ (or 96.39 $\mu_B$/g) at 0°K [14,15].

In a spinel structure, the distribution of cations on site A and B depends on their nature. It strongly influences their magnetic properties and the intensity of X-ray diffraction (XRD) lines.

The characterization of magnetite contained in a silico-aluminous fly ash, after its extraction by magnetic separation, is made by scanning electron microscopy (SEM), transmission electron microscopy (TEM) linked with en-

* Corresponding author. Tel.: +33-03-83-91-24-99; fax: +33-03-83-91-21-66.
*E-mail address*: sandrine.gomes@lcsm.u-nancy.fr (S. Gomes)

0008-8846/99/$ – see front matter 
PII: S0008-8846(99)00133-7

ergy dispersive spectroscopy (EDS), XRD, susceptibility measurements, and $^{57}$Fe Mössbauer spectroscopy.

## 2. Methods

### 2.1. Magnetite separation

The magnetic part of a silico-aluminous fly ash (originating from la Maxe power plant, near Metz in the east of France) is simply extracted by a permanent magnet.

### 2.2. SEM examination, TEM and EDS analyses

The magnetic part of a silico-aluminous fly ash is observed with a scanning electronic microscope (Hitachi S2500). A transmission electron microscope (Philips CM20) operating at 200 keV and equipped with an energy dispersive spectrometer is used to determine the chemical composition of magnetite contained in silico-aluminous fly ash. The magnetic part previously extracted is simply ground and hung in absolute alcohol; then one droplet of the mixture is deposited on a conductive sample grid.

### 2.3. XRD

Powder patterns were recorded from a powder diffractometer with Debye-Scherrer and transmission geometry, equipped with a Mo tube (quartz monochromator, $\theta_m = 6.07°$, $K\alpha_1$ radiation, $\lambda = 0.70930$ Å) and a scintillation detector. Extracted magnetite is put in a silica tube, sealed under vacuum, and heated at 1000°C for 48 h, so that Bragg reflections are better defined and the spectrum more suitable for structural analysis. Peak diffraction of hematite, which is present in low quantity in the sample, disappeared during the heat treatment. The lattice parameter is refined from 16 corrected Bragg peaks position (silicon is used as internal standard) by using UFIT program [16]. Structural analysis is made by using integrated intensities of the Bragg peaks determined by using the PROFIL program [17]. The pseudo-Voigt function was used for modeling the Bragg peak shape, with a reliability factor lower than 5%. Data reduction or structure factors calculation from intensity is made following the formulas: $I(hkl) = m(hkl) \cdot L \cdot P \cdot A \cdot F(hkl)^2$, $L = 1/2 \sin^2\theta \cos\theta$ is the Lorentz factor, $P = (1+\cos^2\theta_m \cos^2 2\theta)/(1+\cos^2\theta_m)$, and $m(hkl)$ multiplicity of Bragg reflection, any absorption correction is applied as it remains approximately constant on the whole analyzed $\theta$ range.

Refinement of the spinel structure is made with the SHELXL97 program [18], mainly used in single crystal studied but also adapted to powder data.

### 2.4. Susceptibility measurements

Susceptibility measurements were performed at room temperature, with a Manics magneto-susceptometer equipped with an electromagnet Drusch, by varying the applied field from 0 to 16 KG.

### 2.5. Mössbauer spectroscopy

The Mössbauer spectrometer comprises a $^{57}$Co/Rh source driven in a sinusoidal mode. Mössbauer spectra are taken at room temperature and fitted with an appropriate superposition of Lorentzian lines. The principal parameters that can be obtained from a Mössbauer spectra are the isomer shift, the quadrupole splitting, the magnetic hyperfine field, and the peak width. The velocity is calibrated with a 25 μm α-Fe foil.

## 3. Results and discussion

### 3.1. TEM and EDS analyses

Three SEM photographs and one characteristic electronic diffraction pattern produced under TEM are shown on Fig. 1.

EDS analyses realized on ten different crystallites are reported on Table 1. Deduced compositions reported to the formula unit $Fe_{(3-x-y-z-t)}Mg_xMn_yCa_zSi_tO_4$ indicate that Fe in magnetite is mainly replaced by Mg and infrequently by Ca, Mn, and Si. The average chemical composition is $Fe_{2.08}Mg_{0.75}Mn_{0.11}Ca_{0.04}Si_{0.02}O_4$.

### 3.2. X-ray diffraction

In Fig. 2, pattern (a) shows a poorly crystallized sample with broad Bragg reflections and pattern (b) is that after heat treatment.

The lattice parameter determined for this spinel structure, $a = 8.3801(15)$ Å, is lower than those of a pure magnetite $Fe_3O_4$ ($a = 8.396$ Å). Observed and calculated interreticular d values are reported on Table 2. $R_{F2} = 0.13$ for all 38 reflections and $R_{F2} = 0.10$ for $F_{obs}^2 > 4\sigma$ (with $R_{F2}$ factor: $R_{F2} = \Sigma \cdot Fobs^2 - Fcal^2 \cdot / \Sigma\ Fobs^2$). This result is in agreement with substitution of $Mg^{2+}$ with a ionic radius of 0.86 Å for $Fe^{2+}$ with a ionic radius of 0.92 Å [19].

The spinel structure of the substituted magnetite found in silico-aluminous fly ash is determined from 38 structure factors and by refining five parameters: one scale factor,

Table 1
Composition of magnetite formed in a silico-aluminous fly ash, expressed in the unit formula unit $Fe_{3-x-y-z-t}Mg_xMn_yCa_zSi_tO_4$ (accuracy ≅ 5%)

| Points measured | Fe | Mg | Mn | Ca | Si |
|---|---|---|---|---|---|
| 1 | 1,722 | 1,046 | 0,157 | 0,032 | 0,042 |
| 2 | 1,988 | 0,850 | 0,123 | 0,028 | 0,010 |
| 3 | 2,141 | 0,727 | 0,102 | 0,015 | 0,014 |
| 4 | 2,424 | 0,490 | 0,0603 | 0,018 | 0,005 |
| 5 | 2,485 | 0,402 | 0,078 | 0,023 | 0,010 |
| 6 | 2,223 | 0,655 | 0,055 | 0,050 | 0,015 |
| 7 | 1,879 | 0,929 | 0,098 | 0,046 | 0,047 |
| 8 | 1,927 | 0,850 | 0,142 | 0,073 | 0,007 |
| 9 | 2,019 | 0,795 | 0,129 | 0,049 | 0,007 |
| 10 | 2,024 | 0,797 | 0,129 | 0,049 | 0,000 |
| Average | 2,08 | 0,75 | 0,11 | 0,04 | 0,02 |

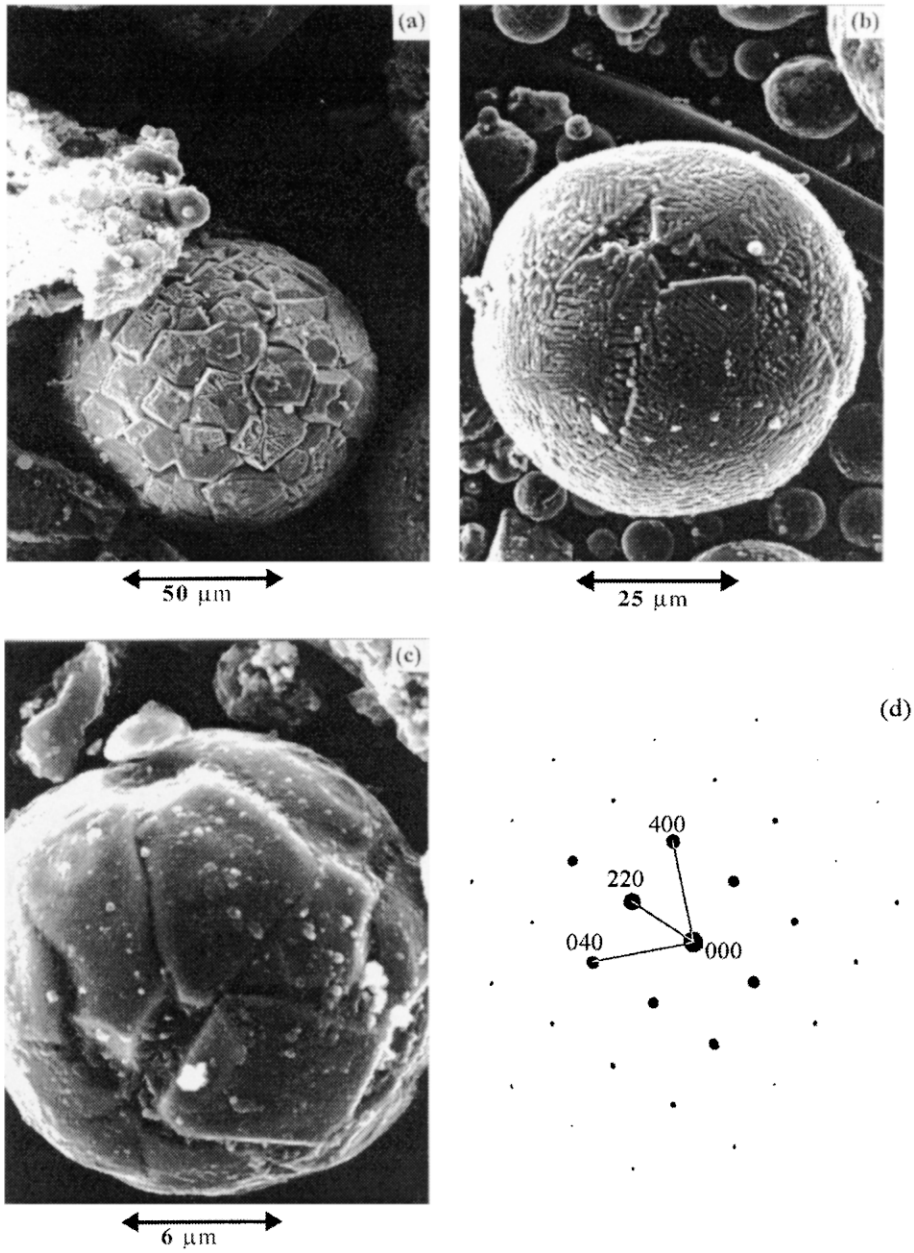


Fig. 1. SEM photographs (a, b, c) and electronic diffraction pattern (MET) along [001] zone axis (d) of silico-aluminous fly ashes covered with magnetite.

one overall temperature factor, the x coordinate of O atoms on 32e site, and mainly occupancy factors of Fe on sites 8a and 16d and Mg on sites 16d. Indeed, a preliminary refinement shows that Mg does not occupy the tetrahedral site 8a. Ca [20] and Si [21] are placed on tetrahedral site 8a and Mn on octahedral site 16d [22] by fixing their occupancy factors at values corresponding to the chemical formula determined above. In order to decrease the number of refined parameters, a constraint is applied assuming that the sum of occupancy factor of Fe, Mg, and Mn on octahedral site is equal to the unity. Moreover, occupancy factor of Fe on the tetrahedral site 8a could be fixed also at the 0.92(−) value. The reliability factor $R_{F2}$ ($F^2 > 4\sigma$) converges satisfactory to 0.10. Observed and calculated structure factors are reported in Table 2 and atomic parameters are summarized in Table 3.

The magnesium content is refined to the 0.73(6) per formula unit, which is in agreement with the chemical composition. These results allow proposition of the substituted magnetite for the following crystallochemical formula: $[Fe^{3+}_{0.92(-)}Ca^{2+}_{0.06(-)}Si_{0.02(-)}]^{tetra}[Fe^{3+}_{1.0(-)}Fe^{2+}_{0.16(-)}Mg^{2+}_{0.73(6)}Mn^{2+}_{0.11(-)}]^{octa}O_{4.0(-)}$.

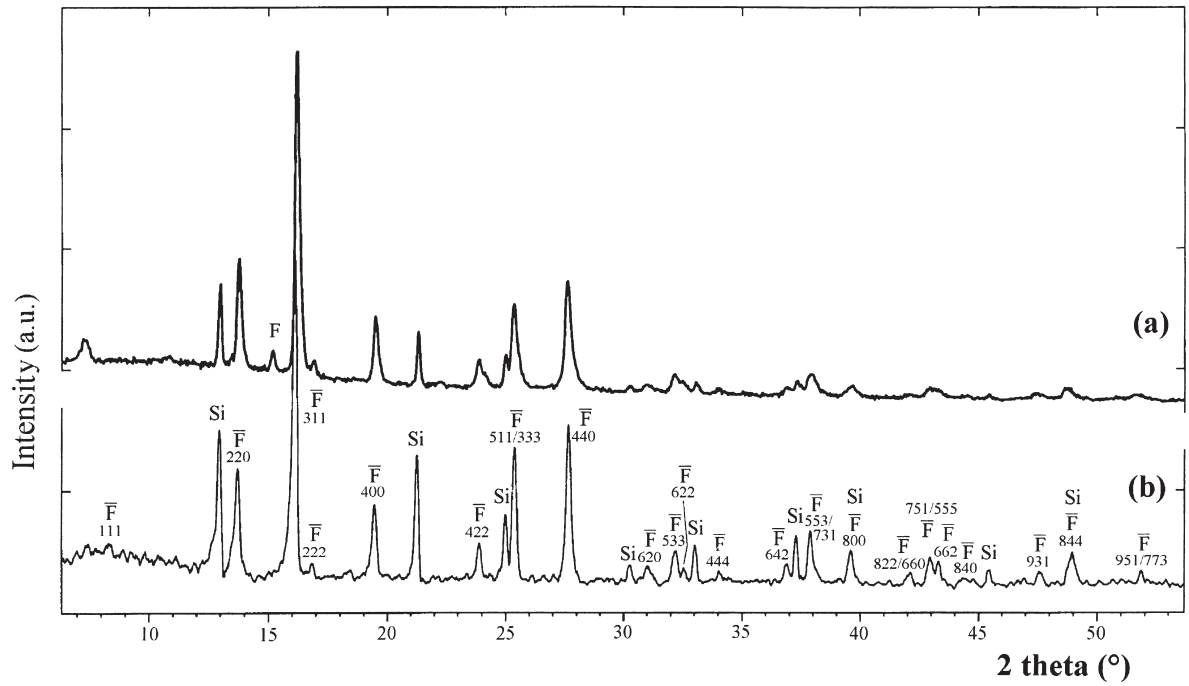


Fig. 2. XRD patterns of the magnetite part of silico-aluminous fly ash (a) before heat treatment, (b) after heat treatment at 1000°C for 48 h. λ = 0.70930 Å, Si = silicon (internal standard), $\overline{F}$ = magnetite, and F = hematite.

### *3.3. Susceptibility measurements*

The curves are presented on Fig. 3. Pure $Fe_3O_4$ is included for comparison.

Magnetic susceptibility curves are characteristic of ferromagnetic behavior. Table 4 reports the magnetization saturation value at room temperature for both compounds. The lower value 39.40 emu/g for magnetite contained in the ash compare to 88.95 emu/g for $Fe_3O_4$ can be explained by the various substitutions shown in the cristallochemical formula expressed above.

A theoretical value $M_s$ corresponding to this crystallochemical formula can be calculated, taking into account that the A and B networks are antiferromagnetically coupled and considering the value of the individual magnetic moment of cations and their position into the structure: $Fe^{3+}$ in A and B, 5 $\mu_B$; $Fe^{2+}$ in B, 4 $\mu_B$; $Ca^{2+}$ and $Si^{4+}$ in A are diamagnetic, $Mn^{2+}$ in B, 5 $\mu_B$; $Mg^{2+}$ in B is diamagnetic. Theoretical magnetization at saturation $M_s$(0 K) is $M_A$-$M_B$, the difference of the moment taken by A and B subnetworks: $M_A = 0.92 \times 5\ \mu_B$ and $M_B = 1.0 \times 5 + 0.16 \times 4 + 0.11 \times 5$. Thus, $M_s$(0 K) = 1.59 $\mu_B$/mole. Since the molar mass corresponding to the formula of magnetite contained in these ashes is 202.92 g, the theoretical $M_s$(0°K) value is 42.9 emu/g. For pure $Fe_3O_4$, the saturation magnetization at room temperature is 92% of its value at 0°K. With the assumption that there is the same decrease for magnetite in the ash, the calculated value at room temperature would be of 39.5 emu/g, identical to the measured value (see Table 4). The crystallochemistry deduced from the structural refinement and analyzed by MET is in agreement with magnetic measurements.

### *3.4. Mössbauer spectroscopy*

Deconvolution of Mössbauer spectra using Lorentzian fit are realized and lead to the results reported on Table 5. The appearance of a six line spectrum (sextet), as shown in Fig. 4, indicates the presence of a long-range magnetically ordered phase, the characteristics of which can be studied afterwards. Because every iron ion makes its own contribu-

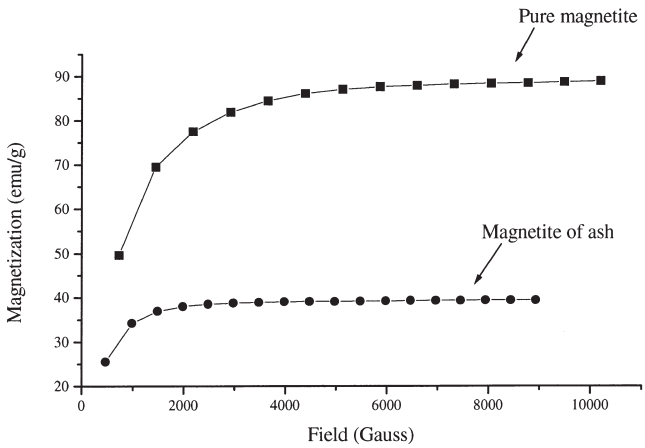


Fig. 3. Magnetization variation (emu/g) of magnetite from silico-aluminous fly ash after heat treatment and of pure magnetite $Fe_3O_4$ under varying magnetic field (Gauss).

Table 2
Observed and calculated distances and structure factors for magnetite formed in silico-aluminous fly ash

| $h^2+k^2+1^2$ | *hkl* | $d_{calc}$(Å) | $d_{obs}$(Å) | $F_{obs}$ | $F_{calc}$ |
|---|---|---|---|---|---|
| 3 | 111 | 4.8382 | 4.8432 | 1 | 0 |
| 8 | 220 | 2.9628 | 2.9627 | 18 | 15 |
| 11 | 311 | 2.5267 | 2.5266 | 64 | 61 |
| 12 | 222 | 2.4191 | 2.4174 | 5 | 3 |
| 16 | 400 | 2.0950 | 2.0946 | 24 | 17 |
| 19 | 331 | 1.9225 | | 0 | 0 |
| 24 | 422 | 1.7106 | 1.7105 | 14 | 19 |
| 27 | 333 | 1.6128 | 1.6124 | 52 | 53 |
| 27 | 511 | 1.6128 | | 0 | 0 |
| 32 | 440 | 1.4814 | 1.4819 | 100 | 100 |
| 35 | 531 | 1.4165 | | 0 | 0 |
| 36 | 442 | 1.3967 | | 0 | 0 |
| 40 | 620 | 1.3250 | 1.3248 | 22 | 14 |
| 43 | 533 | 1.2779 | 1.2776 | 32 | 30 |
| 44 | 622 | 1.2633 | 1.2636 | 9 | 7 |
| 48 | 444 | 1.2096 | 1.2110 | 8 | 9 |
| 51 | 711 | 1.1734 | | 0 | 0 |
| 51 | 551 | 1.1734 | | 0 | 0 |
| 56 | 642 | 1.1198 | 1.1199 | 19 | 21 |
| 59 | 731 | 1.0910 | 1.0914 | 74 | 69 |
| 59 | 553 | 1.0910 | | 0 | 0 |
| 64 | 800 | 1.0476 | | 0 | 0 |
| 67 | 733 | 1.0238 | | 0 | 0 |
| 68 | 644 | 1.0162 | | 0 | 0 |
| 72 | 822 | 0.9876 | 0.9896 | 20 | 13 |
| 72 | 660 | 0.9876 | | 0 | 0 |
| 75 | 555 | 0.9676 | 0.9678 | 52 | 42 |
| 75 | 751 | 0.9676 | | 0 | 0 |
| 76 | 662 | 0.9613 | | 0 | 0 |
| 80 | 840 | 0.9370 | 0.9406 | 37 | 15 |
| 83 | 911 | 0.9198 | | 0 | 0 |
| 84 | 842 | 0.9143 | | 0 | 0 |
| 91 | 931 | 0.8785 | 0.8783 | 25 | 29 |
| 96 | 844 | 0.8553 | 0.8552 | 83 | 72 |
| 99 | 755 | 0.8422 | | 0 | 0 |
| 99 | 771 | 0.8422 | | 0 | 0 |
| 107 | 951 | 0.8101 | 0.8105 | 21 | 24 |
| 107 | 773 | 0.8101 | – | 21 | 14 |

Table 3
Atomic parameters of the impure magnetite (spinel $AB_2O_4$ structure) contained in a silico-aluminous fly ash

| Atoms | Site | Nb at/f.u. |
|---|---|---|
| Fe1 | A(8a) | 0.92(−) |
| Ca | A | 0.06(−) |
| Si | A | 0.02(−) |
| $Fe_2$ | B(16d) | 1.16(1) |
| Mg | B | 0.73(6) |
| Mn | B | 0.11(−) |
| O | 32e, x = 0.249(1) | |

Table 4
Saturation magnetization ($M_s$) of magnetite contained in a silico-aluminous fly ash and comparison with pure $Fe_3O_4$

| | $M_s$ at 295 K (emu/g) | | $M_s$ at 0 K (emu/g) | |
|---|---|---|---|---|
| Pure $Fe_3O_4$ | 88.95 | 3.68 | 96.39 | 4.00 |
| Magnetite in fly ash | 39.40 | 1.46 | 42.9 | 1.59 |

Table 5
Mössbauer parameters for pure magnetite and for magnetite contained in a silico-aluminous fly ash

| Environment | δ (mm/s) | $\Delta E_Q$ (mm/s) | H (kOe) | W (mm/s) | Relative abundance (%) | Interpretation |
|---|---|---|---|---|---|---|
| S1 | 0.68 | 0 | 460 | 0.37 | 63.9 | $[Fe^{2+}Fe^{3+}]^{octa}$ |
| S2 | 0.29 | 0 | 492 | 0.29 | 36.1 | $[Fe^{3+}]^{tetra}$ |
| Magnetite contained in a silico-aluminous fly ash | | | | | | |
| D | 0.16 | 0.1 | | | | Impurity |
| S1 | 0.42 | 0 | 476 | 0.71 | 41.0 | $[Fe^{3+}]^{octa}$ |
| S2 | 0.32 | 0 | 504 | 0.54 | 47.5 | $[Fe^{3+}]^{tetra}$ |
| S3 | 0.72 | 0 | 439 | 0.63 | 9.9 | $[Fe^{2+}]^{octa}$ |

δ, isomer shift relative to metallic iron.

tion to the overall Mössbauer spectrum, the area of each spectral component is approximately proportional to the number of iron in a particular environment. This permits a quantitative determination of the iron content in each site if the Mössbauer f factor is assumed to be the same for all iron sites [23].

In the pure magnetite, $Fe_3O_4$, the iron is situated in the two crystallographically inequivalent tetrahedral A and octahedral B sites [24]. The spectrum of pure magnetite $[Fe^{3+}]^{tetra}[Fe^{3+}, Fe^{2+}]^{octa}O_4$ at room temperature is composed of only two sextets (S1 and S2), characterized by a hyperfine magnetic field H having typical values of 460 and 490 kOe [25], representing 2/3 and 1/3 of the whole spectrum area, respectively. S2 corresponds to $Fe^{3+}$ cations on tetrahedral site while S1 corresponds to $Fe^{2+}$ and $Fe^{3+}$ cations on octahedral site. Supplementary electrons brought by $Fe^{2+}$ are nonlocalized and it can be considered that the octahedral site is occupied by $Fe^{2.5+}$ cations. Such electronic delocalization leads to the appearance of one sextet S1 only; consequently, the two valence states on octahedral sites are not distinct.

The spectrum observed for the ash magnetite is very different. It is composed of three sextets (S1, S2, and S3) with corresponding hyper fine field of 504, 476, and 439 kOe, respectively. S3 sextet is characterized by a higher isomer shift value, about 0.72 and corresponds to $Fe^{3+}$ cations. Here, the electronic mobility is lost or partially lost and leads to the appearance of these three sextuplets, $Fe^{2+}$ on tetrahedral site (S2 representing 47.5% of the whole area), $Fe^{3+}$ on octahedral site (S1 representing 41% of the whole area), and $Fe^{2+}$ on octahedral site (S3 representing 9.9% of the whole area). This phenomena is explained by foreign cations on the octahedral site, and this inhibits electron delocalization confirming the previous results ($Mg^{2+}$ and $Mn^{2+}$ on octahedral site).

The cation distribution deduced from these measurement is the following: 48% of the whole iron atoms are $Fe^{3+}$ on

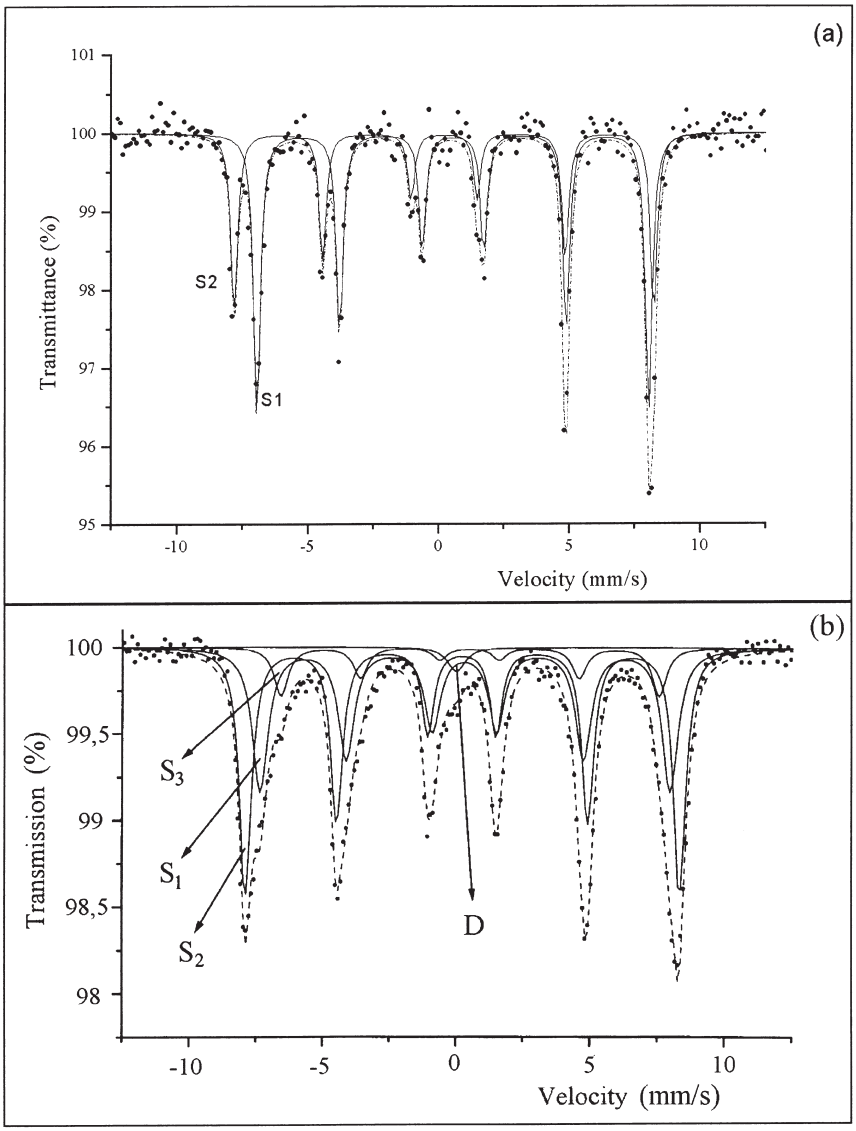


Fig. 4. Mössbauer spectra of pure magnetite (a) and those contained in the silico-aluminous fly ash (b).

tetrahedral site, so 52% of iron are on octahedral site, of which 42% are $Fe^{3+}$ and 10% are $Fe^{2+}$. The $[Fe]^{octa}/[Fe]^{tetra}$ ratio is 1.1, a value very near of 1.26 deduced from the cristallochemical formula refined before. Mössbauer results confirm that the substitution occurs mainly on the octahedral site of the spinel structure.

## 4. Conclusions

TEM linked with EDS analysis allowed us to determine the following chemical formula for the impure magnetite contained a silico-aluminous fly ash: $Fe_{2.08}Mg_{0.75}Mn_{0.11}Ca_{0.04}Si_{0.02}O_4$.

Structural refinement and also lattice parameter led to the knowledge of cation distribution on the octahedral and tetrahedral sites of the spinel structure. It has been summarized in the following cristallochemical formula: $[Fe^{3+}_{0.92(-)}Ca^{2+}_{0.06(-)}Si_{0.02(-)}]^{tetra}[Fe^{3+}_{1.0(-)}Fe^{2+}_{0.16(-)}Mg^{2+}_{0.73(6)}Mn^{2+}_{0.11(-)}]^{octa}O_{4.0(-)}]$.

These formulas are compatible with magnetic measurements and Mössbauer spectroscopy. It confirms that substitution occurs mainly on octahedral site.

Magnesium contained in a silico-aluminous fly ash is mainly incorporated in inert spinel phase and so does not contribute to the reactivity of these residues.

## Acknowledgments

This study is a part of the contract between University Henri Poincaré from Nancy and EDF (Electricité de France), contract no. MX1502. SEM and microprobe analyses were conducted by A. Kohler from the Service Commun d'Analyses par Sondes Electroniques; TEM analyses were conducted by J. Ghanbaja from the Service Commun de Mi-

croscopie Electronique par Transmission; and susceptibility measurements were conducted by R. Welter from Laboratoire de Chimie du Solide Minéral, from the Faculty of Sciences, Vandoeuvre les Nancy (France).

## References

[1] M. Regourd, 8th ICCC, Rio de Janeiro, Brazil, Abla Gráfica e Editora, Vol. I, 1986, pp. 200–229.
[2] F.M. Lea, The Chemistry of Cement Concrete, Edward Arnold Ltd, London, 1970.
[3] H. Pietersen, A.L.A. Fraay, J. Bijen, Reactivity of fly ash at high pH, Mat Res Soc Symp Proc 178 (1990) 139.
[4] J.C. Qian, E.E. Lachowski, F.P. Glasser, Microstructure and chemical variation in class F fly ash glass, Mat Res Symp Proc 113 (1988) 45.
[5] M. Venuat, Adjuvants et Traitements, M. Venuat, Paris, 1984.
[6] J.C. Qian, E.E. Lachowski, F.P. Glasser, The microstructure of National Bureau of standards reference fly ashes, Mat Res Soc Symp Proc 136 (1989) 77.
[7] C.L. Kilgour, K.L. Bergeson, S. Schlorholtz, Storage alternatives for high-calcium fly ashes, Mat Res Soc Symp Proc 136 (1989) 161.
[8] M.M. Alasali, V.M. Malhotra, Role of concrete incorporating high volumes of fly ash in controlling expansion due to alkali-aggregate reaction, ACI Mat J 88 (2) (1991) 159.
[9] S. Diamond, On the glass present in low-calcium and in high-calcium flyashes, Cem Concr Res 13 (1983) 459.
[10] G.J. McCarthy, D.M. Johansen, S.J. Steinwand, X-ray powder diffraction study of NBS fly ash standard reference materials, Adv X-Ray Anal 31 (1988) 331.
[11] G.J. McCarthy, K.J. Solem, X-ray diffraction of fly ash. II. Results, Adv X-Ray Anal 34 (1991) 387.
[12] G.J. McCarthy, X-ray powder diffraction for studying the mineralogy of fly ash, Mat Res Soc Symp Proc 113 (1988) 75.
[13] S. Gomes, M. François, Characterization of mullite in silico-aluminous fly ash by XRD, TEM and $^{29}$Si MAS NMR, Cem Concr Res (in press).
[14] D.R. Lide, Handbook of Chemistry and Physics, CRC Press, 74th Ed., London, 1994.
[15] C.G. Shull, E.O. Wollan, W.C. Koehler, Neutron scattering and polarization by ferromagnetic materials, Phys Rev 84 (1951) 912.
[16] M. Evain, UFIT program V1.3, Institut des Matériaux de Nantes, Nantes, France, 1992.
[17] Programme PROFILE pour Diffrac-at, socabim, Paris, France.
[18] G.M. Sheldrick, Program ShelXL97 for the refinement of Crystal Structure, University of Göttingen Germany, 1997.
[19] F.G. Fumi, M.P. Tosi, Ionic sizes and born repulsive parameters in the NaCl-type alkali halides—I, J Phys Chem Solids 25 (1964) 31.
[20] R. Gérardin, A. Bonazebi, E. Million, J.F. Brice, O. Evrard, J.P. Sanchez, Etude des magnétites dopées à la chaux: Substitution du fer par le calcium en site tétraédrique, J Solid State Chem 78 (1989) 154.
[21] N.G. Newberry, D.R. Peacor, E.J. Essene, J.W. Geissman, Silicon in magnetite: High resolution microanalysis of magnetite-illmenite inter growths, Contrib Mineral Petrol 80 (1982) 334.
[22] G.A. Sawartzky, F. Van Der Woude, A.H. Morrish, Recoilless—Fraction ratios for $Fe^{57}$ in octahedral and tetrahedral sites of a spinel and a garnet, Phys Rev 183 (1969) 383.
[23] E. Murad, J.H. Johnston, Mössbauer spectroscopy applied to inorganic chemistry, in: G. J. Long (Ed.), 2, Plenum, New York, 1987, pp. 507.
[24] P.S. Sidhu, R.J. Gilkes, A.M. Posner, The synthesis and some properties of Co, Ni, Zn, Cu, Mn and Cd substituted magnetites, J Inorg Nucl Chem 40 (1978) 429.
[25] J.M. Daniels, A. Rosencwaig, Mössbauer spectroscopy of stoichiometric and non-stoichiometric magnetite, J Phys Chem Solids 30 (1969) 1561.